

# Modeling of Molecular Weight Distribution of Gas-Phase Polymerization of Butadiene

Dongyu Fang, Jianzhong Sun, Qiyun Zhou

Department of Chemical Engineering, Zhejiang University, Hangzhou 310027, People's Republic of China

Received 10 April 2002; accepted 5 May 2002

**ABSTRACT:** A mathematical model of the molecular weight distribution (MWD) based on a multilayer model and an improved intrinsic kinetics model was proposed to simulate the MWD of the gas-phase polymerization of butadiene with a heterogeneous catalyst. Intrinsic kinetics and heat and mass-transfer resistances based on the multilayer model of a polymeric particle were considered in the modeling of the MWD. The effects of the reaction conditions, catalyst particle size, mass-transfer resistance, deactivation of active sites, and transfer of the polymer chain on the molecular weight and MWD were simulated. The results

show that the effects of the deactivation of active sites and transfer of the polymer chain on the average molecular weight are significant and that the effect of the catalyst particle size on the MWD is not significant. The simulation results of the molecular weight and MWD are compared with the experimental results. © 2003 Wiley Periodicals, Inc. *J Appl Polym Sci* 88: 88–103, 2003

**Key words:** molecular weight distribution/molar mass distribution; modeling; simulations

## INTRODUCTION

Gas-phase polymerization of butadiene catalyzed by heterogeneous catalysts has been of increasingly interest in recent years. Several patents describing catalysts for gas-phase polymerization of butadiene have been published.<sup>1–3</sup> Eberstein et al.<sup>4</sup> and Zhao et al.<sup>5</sup> studied the effect of the operation conditions on the kinetics of polymerization in a model reactor. Garmatter<sup>6</sup> and Sun et al.<sup>7,8</sup> proposed models for this process and for particle growth using a multilayer model. Zhao et al.<sup>9,10</sup> also constructed a model based on the multi-grain model to simulate the particle growth and morphology in the gas-phase polymerization of butadiene. To date, no articles dealing with the modeling of the molecular weight distribution (MWD) of the gas-phase polymerization of butadiene based on the multilayer model have been published.

The object of this article was the development of a mathematical model based on a multilayer model, which can be used to simulate the MWD of the gas-phase polymerization of butadiene with a heterogeneous catalyst. An improved intrinsic kinetic model, weight distribution function, and numerical solution technique are proposed. The simulations include mainly the effects of the reaction conditions, mass-

transfer resistance, and catalyst particle size on the average molecular weight and MWD.

## EXPERIMENTAL

A heterogeneous rare-earth catalyst, whose main catalyst was neodymium–triethyl and cocatalyst was triethylaluminum, was used in the experiment.<sup>11</sup> The mol ratio of aluminum and neodymium was 33. The catalyst was loaded on silica gels (SiO<sub>2</sub> 955).

The experimental apparatus is shown in Figure 1. The polymerization was carried out in a horizontal agitating bed reactor made of stainless steel. The self-cleaning agitator with double axes was used to prevent polybutadiene particles from agglomerating. Monomer (butadiene) must be treated with KOH and an Al<sub>2</sub>O<sub>3</sub> molecular sieve to remove the polymerization inhibitor and trace H<sub>2</sub>O, respectively, before use. A Ag molecular sieve (the argentum content is 28%) and an Al<sub>2</sub>O<sub>3</sub> molecular sieve were used to remove trace O<sub>2</sub> and trace H<sub>2</sub>O in the inert gas (argon), respectively.

The reactor was dried at 120°C for several hours to eliminate trace H<sub>2</sub>O. The argon gas was used as a replacement gas to carry the vapor of trace H<sub>2</sub>O out of the reactor.

The dispersing medium (SiO<sub>2</sub> powder) was charged into the reactor before the addition of the catalyst. It must be dried under 400°C for 24 h to eliminate adsorbed water prior to addition. Since there are many hydroxyl groups on the surface of the SiO<sub>2</sub> particles, the dispersing medium must first deal with the alkyl aluminum; otherwise, they will deactivate the catalyst.

Correspondence to: J. Sun.

Contract grant sponsor: National Natural Science Foundation of China; contract grant number: 29876035.

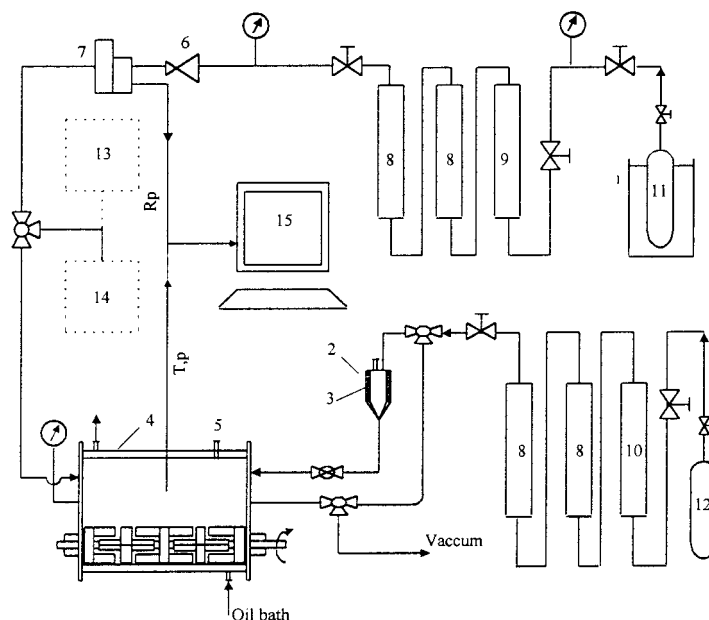


**Figure 1** Schematic of butadiene gas-phase polymerization system: (1) thermostat bath; (2) equipment for adding inert powder; (3) heater; (4) stirred-bed reactor; (5) inlet for catalyst; (6) pressure regulator; (7) mass flowmeter; (8) activated aluminum oxide; (9) KOH; (10) Mn molecular sieves; (11) butadiene; (12) Ar gas; (13) trace amounts of oxygen analyzer; (14) trace amounts of water analyzer; (15) computer.

The catalyst was then fed to the reactor under the protection of argon.

Operating parameters, such as the reaction temperature, reaction pressure, and mass flow of butadiene, were measured by a temperature sensor, a pressure sensor, and a trace gas flowmeter, respectively, monitored online by a computer. As the reaction progressed, the concentration of the monomer in the reactor decreased. To keep the pressure invariable, butadiene gas was flowed into the reactor continuously. The mass of gas flowing into the reactor in a specific time was equal to the consuming rate of the monomer.

The experiment was carried out under the conditions shown in Table I.<sup>12</sup> In the experiment, the kind of catalyst, the properties of the catalyst, and the kind of dispersing medium are much different from those in the experiment of Zhao.<sup>5</sup> So, the kinetic behaviors are not the same as before. The kinetic curves are shown in Figures 2 and 3.

The product (polybutadiene) was dissolved by THF. The measurement of the average molecular weight

and the MWD were carried out by a Waters 150C gel permeation chromatograph (GPC) at 30°C. Under this condition, the value of  $K$  was 0.0076 mL/g and the value of  $\alpha$  was 0.68.<sup>5</sup>

### MULTILAYER MODEL OF POLYMER PARTICLE

Sun et al. used the multilayer to simulate the particle growth in the gas-phase polymerization of butadiene.<sup>7</sup> The simulation results predict that the resistance of heat transfer can be neglected because the temperature profile in the polymeric particle is almost uniform and

**TABLE I**  
Reaction Conditions of Gas-phase Polymerization of Butadiene

Reaction pressure ( $p$ )	0.65–1.4 atm
Reaction temperature ( $T$ )	30–50°C
Concentration of monomer gas ( $M_{\text{gas}}$ )	0.026–0.054 mol/L
Initial concentration of active sites ( $C_0^*$ )	$2.418 \times 10^{-5}$ mol Nd/g Cat
Dispersing medium	SiO <sub>2</sub>

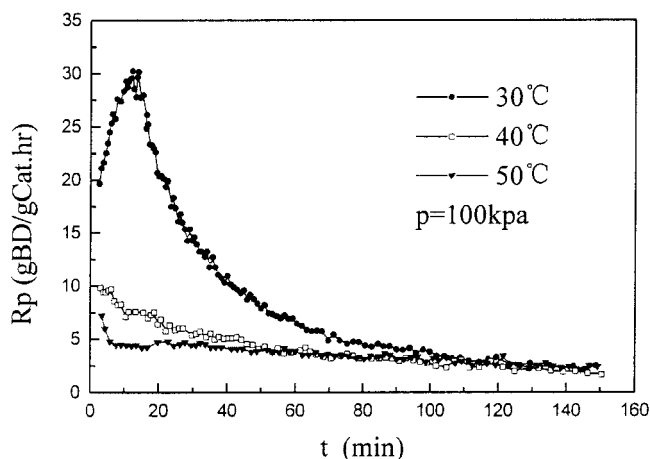


**Figure 2** Effect of reaction temperature on polymerization rate at 100 kPa.

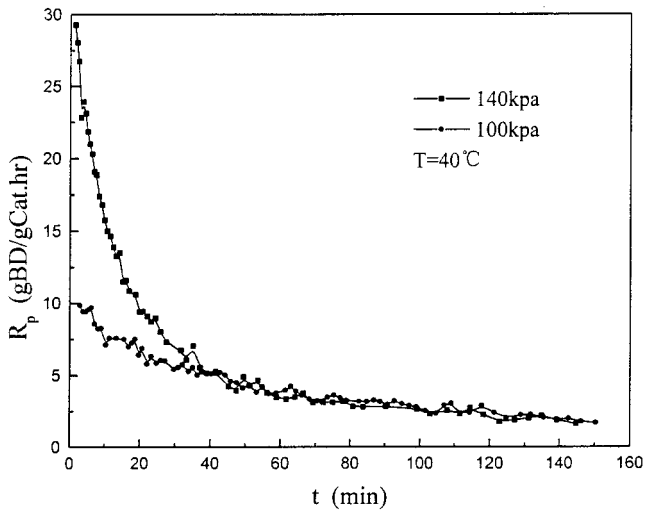


**Figure 3** Effect of reaction pressure on polymerization rate at 40°C.

the mass-transfer limitation is significant. Soares and Hamielec simulated the chain-length distribution of the gas-phase copolymerization of olefin monomers on the basis of the multilayer model.<sup>13</sup> Zhao et al. used the multigrain model to simulate the particle growth and morphology in the gas-phase polymerization of butadiene.<sup>9,10</sup> Although the multigrain model can give good computational results of the particle growth and morphology, it is too complicated to be used in the simulation of the MWD of the gas-phase polymerization of butadiene. The multilayer model is better to

simulate the MWD in this case. The boundary conditions of the multilayer model here are somewhat different from those of the multilayer model used before. A schematic graph of the multilayer model is shown in Figure 4.<sup>10</sup>

In the multilayer model, the polymeric particle is divided into several concentric spherical layers. Every layer is the uniform body. The monomer, active sites, and polymers are dispersed in it. There are no micro-particles in every layer, which is not the same as in the multigrain model.

At the beginning of the reaction, the concentration of active sites in each layer is the same. The catalyst particle becomes the polymer particle immediately after the beginning of the reaction. The polymer chains are produced in the layers, which makes the particle layers grow.

The mass balance of the monomer can be described by the following diffusion-reaction equations:

$$\frac{\partial M(r, t)}{\partial t} = \frac{D_e}{r^2} \frac{\partial}{\partial r} \left( r^2 \frac{\partial M}{\partial r} \right) - R_p \quad (1)$$

$$\text{I.C. } M(r, 0) = 0 \quad (2)$$

$$\text{B.C. } \frac{\partial M(0, t)}{\partial t} = 0 \quad (3)$$

$$M(R, t) = M_p \quad (4)$$

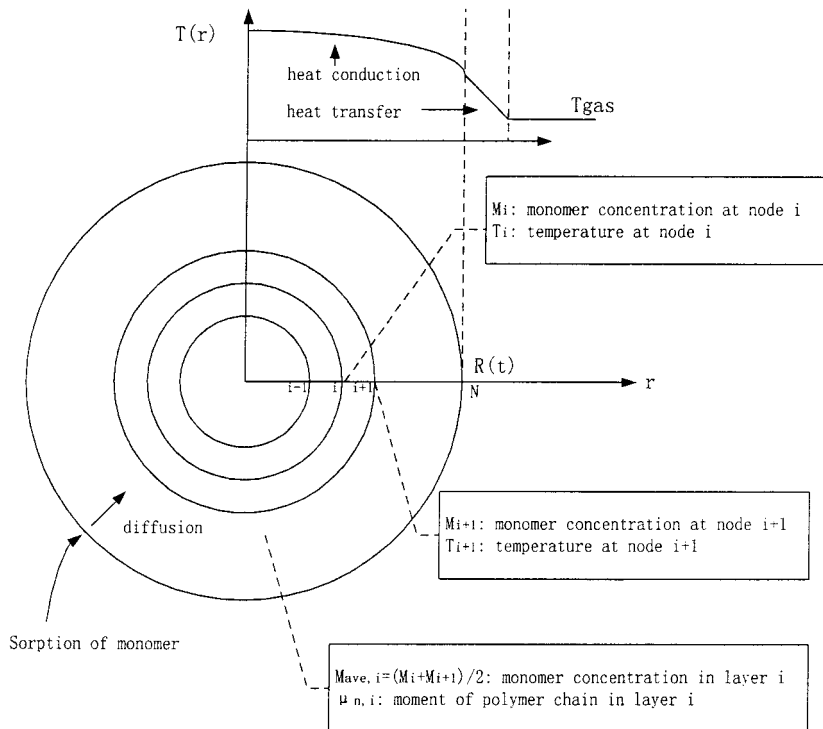


**Figure 4** Scheme of polymeric multilayer model.

The energy-balance equations are shown as the following:

$$\rho_p C_p \frac{\partial T(r, t)}{\partial t} = \frac{k_e}{r^2} \frac{\partial}{\partial r} \left( r^2 \frac{\partial T}{\partial r} \right) - (-\Delta H_p) R_p \quad (5)$$

$$\text{I.C. } T(r, 0) = T_{\text{gas}} \quad (6)$$

$$\text{B.C. } \frac{\partial T(0, t)}{\partial r} = 0 \quad (7)$$

$$k_e \frac{\partial T(R, t)}{\partial r} = h [T_{\text{gas}} - T(R, t)] \quad (8)$$

The polymerization rate  $R_p$  is calculated using the average concentration of the monomer of each layer. Since the polymeric particle is growing during the polymerization, the volume of every layer must be updated according to the amount of polymer produced in each time interval.

The updating equations can be expressed as

$$V_i^0 = \frac{4\pi}{3} [(r_{i+1}^0)^3 - (r_i^0)^3] \quad (9)$$

$$V_i^{k+1} = V_i^k \left[ \frac{R_p MW \Delta t}{\rho_p} + 1 \right] \quad (10)$$

$$r_{i+1}^{k+1} = \left[ \frac{3}{4\pi} V_i^{k+1} + (r_i^{k+1})^3 \right]^{1/3} \quad (11)$$

The monomer concentration and temperature at each node were calculated by the three-point Lagrangian interpolation polynomial method. L'Hôpital's rule<sup>10</sup> was used for the situation at the center of the polymer particle. Then, the radial profile of the monomer concentration and temperature can be described as follows:

$$\begin{aligned} \frac{dM(r_i)}{dt} = 2D_e [A_i M(r_{i-1}) + B_i M(r_i) + C_i M(r_{i+1}) \\ - R_p(r_i) \quad i = 2 \dots N - 2 \end{aligned} \quad (12)$$

$$\frac{dM(r_0)}{dt} = D_e [B_0 M(r_0) - B_0 M(r_1)] - R_p(r_0) \quad (13)$$

$$\begin{aligned} \frac{dT(r_i)}{dt} = 2 \frac{k_e}{C_p \rho_p} [A_i T(r_{i-1}) + B_i T(r_i) + C_i T(r_{i+1}) \\ - \frac{(-\Delta H_p R_p)}{C_p \rho_p} \quad i = 2 \dots N - 3 \end{aligned} \quad (14)$$

$$\frac{dT(r_0)}{dt} = \frac{k_e}{C_p \rho_p} [B_0 T(r_0) - B_0 T(r_1)] - \frac{(-\Delta H_p R_p)}{C_p \rho_p} \quad (15)$$

$$\begin{aligned} \frac{dT(r_{N-1})}{dt} = \frac{2k_e}{C_p \rho_p} \left\{ \frac{r_{N-2}}{r_{N-1}(r_{N-1} - r_{N-2})^2} T(r_{N-2}) \right. \\ \left. - \left[ \frac{r_{N-2}}{r_{N-1}(r_{N-1} - r_{N-2})^2} + \frac{h}{k_e(r_{N-1} - r_{N-2})} \right] T(r_{N-1}) \right\} \\ + \frac{-\Delta H_p R_p}{C_p \rho_p} \quad (16) \end{aligned}$$

$$A_i = \frac{2r_i - r_{i+1}}{r_i(r_{i-1} - r_i)(r_{i-1} - r_{i+1})} \quad (17)$$

$$B_i = \frac{3r_i - r_{i+1} - r_{i-1}}{r_i(r_i - r_{i-1})(r_i - r_{i+1})} \quad (18)$$

$$C_i = \frac{2r_i - r_{i-1}}{r_i(r_{i+1} - r_{i-1})(r_{i+1} - r_i)} \quad (19)$$

$$B_0 = -\frac{6}{(r_1 - r_0)^2} \quad (20)$$

The intrinsic kinetics should be considered for the modeling of the MWD, which is not the same as the kinetic model used in the multilayer model of Sun et al.<sup>10</sup> At the beginning of the reaction, a sorption process would occur. This makes the boundary condition of the concentration of the monomer not the same as that of the bulk concentration of the monomer gas, differing from the assumption of Soares and Hamielec and Sun et al. After the sorption process, the monomer will diffuse into the particle and the reaction will take place. The boundary condition must be calculated using sorption equations, which will be shown later.

In eq. (8),  $h$  is the heat-transfer coefficient given by the Ranz–Marshall correlation, which can be used to describe the heat transfer at the external layer<sup>7,14</sup>:

$$Nu = 2 + 0.6Re^{1/2}Pr^{1/2} \quad (21)$$

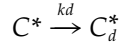
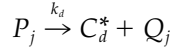
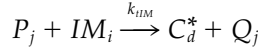
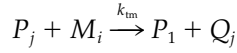
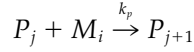
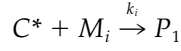
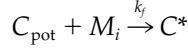
where  $Nu$  is the Nusselt number  $hd_p/k_{\text{gas}}$ ;  $Re$ , the Reynold's number,  $\rho_{\text{gas}}ud_p/\mu_{\text{gas}}$ ; and  $Pr$ , the Prandtl number,  $\mu_{\text{gas}}C_{p\text{gas}}/k_{\text{gas}}$ .

Using the multilayer model introduced above, the monomer concentration and the temperature at each node are obtained, which is important to calculate the MWD of each layer of the polymeric particle. The calculation method of the average concentration of the monomer in each layer is shown in Figure 4. Besides the distribution of the monomer concentration, to further the modeling of the MWD of gas-phase polymerization, constructing the suitable intrinsic kinetics model is an important step.

#### INTRINSIC KINETICS MODEL

The reaction kinetics mechanism considered here includes mainly site formation, initiation, propagation,

transfer to the monomer, transfer to the impurities, and deactivation of the living polymers and active sites, as follows:



where  $C_{\text{pot}}$  is the concentration of potential active sites of a catalyst and they must react with a monomer to format the active sites;  $C^*$ , the concentration of an active site;  $M_i$ , the average concentration of the monomer in the  $i$ th layer;  $P_j$  and  $Q_j$ , the concentration of the living polymer and the dead polymer, respectively; and  $IM_i$ , the concentration of impurities in the  $i$ th layer. Since the reactor must be cleaned before the reaction, the concentration of an impurity in the reactor is so low that it could be considered negligible. For polymerization of polyolefins using heterogeneous catalysts, their MWDs are broad. For example, their polydispersing index ( $PI$ ) range is from 4 to 20 or even broader.<sup>15</sup> Some researchers have found that multiactive sites will lead to a wide MWD ( $PI \gg 2$ ).<sup>15,16</sup> In this article, the MWD of the gas-phase polymerization of butadiene is relatively narrow. From the experiment result, the  $PI$  of the gas-phase polymerization of butadiene is about 2.<sup>12</sup> So, only one kind of active site is considered here. At the same time, there are many kinds of factors that can affect the deactivation reaction. All of them can be concluded in the  $kd$ . In addition, kinetic research has found that the deactivation reaction approached being a first-order reaction.<sup>12</sup> To simplify the problem, a first-order deactivation reaction mechanism is assumed.

A series of equations can be expressed to describe the system of the gas-phase polymerization of butadiene:

$$\frac{dC_{\text{pot}}}{dt} = -k_f M_i C_{\text{pot}} \quad (22)$$

$$\frac{dC^*}{dt} = k_f M_i C_{\text{pot}} - k_i M_i C^* - k_d C^* \quad (23)$$

$$\frac{dP_{\text{act}}}{dt} = k_i C^* M_i - k_d P_{\text{act}} - k_{\text{tm}} P_{\text{act}} M_i \quad (24)$$

$$P_{\text{act}} = \sum_{j=1}^{\infty} P_j \quad (25)$$

When  $t = 0$ ,

$$C_{\text{pot}}(0) = C_0^* \quad (26)$$

$$C^*(0) = 0 \quad (27)$$

$$P_{\text{act}}(0) = 0 \quad (28)$$

The equation of the reaction rate is

$$R_p = k_p M_i P_{\text{act}} \quad (29)$$

Equation (29) is then solved simultaneously with eqs. (22)–(28) to get the intrinsic kinetics as follows:

$$R_p = \frac{k_p k_i k_f M^3 C_0^*}{k_i M - k_f M + k_d} \left[ \frac{e^{-k_f M t}}{\alpha} - \frac{e^{-(k_d + k_i M)t}}{\beta} + \frac{e^{-(k_d + k_{\text{tm}} M)t}}{\gamma} \right] \quad (30)$$

$$\alpha = k_d + k_{\text{tm}} M - k_f M \quad (31)$$

$$\beta = k_{\text{tm}} M - k_i M \quad (32)$$

$$\gamma = \frac{k_i M + k_d - k_f M}{(k_{\text{tm}} M - k_i M)(k_d + k_{\text{tm}} M - k_f M)} \quad (33)$$

Since the sorption process will occur instantly at the beginning of the reaction, the monomer concentration at the surface of the particle is the sorption concentration of the monomer, not the bulk concentration of the monomer gas. The concentration of the monomer in eq. (30) is much higher than is the calculated bulk concentration of the monomer gas. The sorption concentration of the monomer can be obtained using eqs. (34) and (35)<sup>9,17</sup>:

$$S = \frac{M_p}{p} = k_D e^{\delta M_p} \quad (34)$$

$$S = \frac{M_p}{p} = S_0 e^{-\Delta H_s/RT} \quad (35)$$

Zhao et al. calculated some sorption concentrations at different reaction conditions of the gas-phase polymerization of butadiene.<sup>5</sup>  $M_p$  is the sorption concentration of the monomer and  $p$  is the reaction pressure. By using the model to fit the kinetic curves obtained in the experiment, the kinetic constants in the model equation can be obtained.

### MWD MODEL

The  $n$ th moment of the generic distribution  $f(j)$  is defined by the equation

$$\mu_n = \sum_{j=1}^{\infty} j^n f(j) \quad (36)$$

In the case of the gas-phase polymerization of butadiene,  $f(j)$  is the concentration of the living polymer or dead polymer and  $j$  is the degree of polymerization.  $\mu_n^a$  and  $\mu_n^d$  are  $n$ th moment of the living and dead polymers, respectively.

From the mechanism of kinetics and population balance, the balance equation of the living polymer and the dead polymer can be solved to get the moment equations of the living and dead polymers:

$$\frac{dP_1}{dt} = k_i C^* M - k_p P_j M - k_d P_1 \quad (37)$$

$$\frac{dP_j}{dt} = k_p P_{j-1} M - k_p P_j M - k_{tm} P_j M - k_d P_j \quad (38)$$

$$\frac{dQ_j}{dt} = k_{tm} P_j M + k_d P_j \quad (39)$$

The population balance for all chains of the living polymer can be obtained by summing eq. (38) from  $j$  equal to 2 to infinity plus eq. (37). On the other hand, the population balance for the dead polymer of all chain lengths is obtained by summing eq. (39) from  $j$  equal to 2 to infinity. In fact, these are the differential equations of the zero moment of the living and dead polymers:

$$\frac{d\mu_0^a}{dt} = \frac{k_i k_f M^2 C_0^*}{k_i M - k_p M + k_d} [e^{-k_p M t} - e^{-(k_i M + k_d) t}] - k_d \mu_0^a \quad (40)$$

$$\frac{d\mu_0^d}{dt} = (k_{tm} M + k_d)(\mu_0^a - P_1) \quad (41)$$

$$\mu_0^a = \sum_{j=1}^{\infty} P_j \quad (42)$$

$$\mu_0^d = \sum_{j=2}^{\infty} Q_j \quad (43)$$

The first and second moments of the living polymer are obtained by multiplying eq. (38) by  $j$  and  $j^2$ , respectively, and summing from 2 to infinity plus eq. (37). It is the same with the dead polymer:

$$\frac{d\mu_1^a}{dt} = (k_p M + k_{tm} M) \mu_0^a - (k_{tm} M + k_d) \mu_1^a + k_i C^* M \quad (44)$$

$$\frac{d\mu_2^a}{dt} = (k_p M + k_{tm} M) \mu_0^a + 2k_p M \mu_1^a - (k_d + k_{tm} M) \mu_2^a + k_i C^* M \quad (45)$$

$$\frac{d\mu_1^d}{dt} = (k_{tm} M + k_d)(\mu_1^a - P_1) \quad (46)$$

$$\frac{d\mu_2^d}{dt} = (k_{tm} M + k_d)(\mu_2^a - P_1) \quad (47)$$

$$\mu_1^a = \sum_{j=1}^{\infty} j P_j \quad (48)$$

$$\mu_2^a = \sum_{j=1}^{\infty} j^2 P_j \quad (49)$$

$$\mu_1^d = \sum_{j=2}^{\infty} j Q_j \quad (50)$$

$$\mu_2^d = \sum_{j=2}^{\infty} j^2 Q_j \quad (51)$$

Equations (40)–(51) are solved with eqs. (37)–(39) simultaneously. The moments of the polymer chains will be obtained. Here, all the living chains are assumed to have the same activity. From the moments, the average molecular weight of each layer can be estimated.  $MW$  is the molecular weight of butadiene:

$$\bar{M}_{n,i} = \frac{\mu_{1,i}^a + \mu_{1,i}^d}{\mu_{0,i}^a + \mu_{0,i}^d} MW \quad (52)$$

$$\bar{M}_{w,i} = \frac{\mu_{2,i}^a + \mu_{2,i}^d}{\mu_{1,i}^a + \mu_{1,i}^d} MW \quad (53)$$

**TABLE II**  
Thermal, Physical, and Transport Properties  
of Gas-phase Polymerization of Butadiene

Property	Value	Reference
$C_0^*$ (mol Nd/g Cat)	$2.418 \times 10^{-5}$	13
$C_p$ (J kg <sup>-1</sup> K <sup>-1</sup> )	1600	9
$k_e$ (W m <sup>-1</sup> K <sup>-1</sup> )	0.15	9
$C_{pgas}$ (J kg <sup>-1</sup> K <sup>-1</sup> )	1681	9
$D_e$ (m <sup>2</sup> /s)	$10^{-11}$ – $10^{-9}$	9
$\Delta H_p$ (J/mol)	73,000	9
$R_{cat}$ ( $\mu$ m)	10–50	9
$k_{gas}$ (W m <sup>-1</sup> K <sup>-1</sup> )	0.015–0.021	9
$S_0$ [L(STP) L <sup>-1</sup> polymer atm <sup>-1</sup> ]	$4.5 \times 10^{-3}$	7
$k_D$ [L (STP) L <sup>-1</sup> polymer Pa <sup>-1</sup> ]	$(9.2$ – $11.25) \times 10^{-5}$	7
$\delta$ [L polymer/L (STP)]	$(8.55$ – $10.18) \times 10^{-3}$	7
$\Delta H_s$ (kJ/mol)	–14.4	7
$\rho_p$ (kg/m <sup>3</sup> )	890	9
$\rho_{gas}$ (kg/m <sup>3</sup> )	4.108–5.4246	9
$\rho_{cat}$ (kg/m <sup>3</sup> )	623	9

$$PI_i = \frac{\bar{M}_{n,i}}{M_{w,i}} \quad (54)$$

The weight-distribution function is used here to get the MWD:

$$P_{3,i} = e^{-(k_p M + k_{tm} M + k_d)t} A (k_p M)^2 \left[ \frac{K_1}{k_p M + k_{tm} M + k_d - k_f M} e^{(k_p M + k_{tm} M + k_d - k_f M)t} - \frac{K_2}{k_p M + k_{tm} M - k_i M} e^{(k_p M + k_{tm} M - k_i M)t} - \frac{K_3}{k_p M + k_{tm} M + k_d} e^{(k_p M + k_{tm} M + k_d)t} - Kt - \left( \frac{K_1}{k_p M + k_{tm} M + k_d - k_f M} - \frac{K_2}{k_p M + k_{tm} M - k_i M} - \frac{K_3}{k_p M + k_{tm} M + k_d} \right) \right] \quad (59)$$

$$P_{j,i} = (k_p M)^{j-1} \left\{ \frac{K_1}{(k_p M + k_{tm} M + k_d - k_f M)^{j-2}} e^{-k_f M t} + \frac{K_2}{(k_p M + k_{tm} M - k_i M)^{j-2}} e^{-(k_d + k_i M)t} - \frac{K_3}{(k_p M + k_{tm} M)^{j-2}} e^{-k_d t} - \frac{K_4}{(j-1)!} t^{j-1} - \frac{K_1 + K_2 - K_3}{(j-2)!} t^{j-2} - \left( \frac{K_2}{(k_p M + k_{tm} M - k_i M)^{j-2}} - \frac{K_1}{(k_p M + k_{tm} M + k_d - k_f M)^{j-2}} + \frac{K_3}{(k_p M + k_{tm} M)^{j-2}} - \sum_{m=1}^{j-3} \left[ \frac{K_1}{(k_p M + k_{tm} M + k_d - k_f M)^{j-2}} + \frac{K_2}{(k_p M + k_{tm} M - k_i M)^{j-2}} - \frac{K_3}{(k_p M + k_{tm} M)^{j-2}} \right] \frac{t^{j-2-m}}{(j-2-m)!} \right) \right\} \quad j \geq 4 \quad (60)$$

$$F_{w,i}(j) = \frac{jP_{j,i} + jQ_{j,i}}{\sum_{j=1}^{\infty} jP_{j,i} + \sum_{j=2}^{\infty} jQ_{j,i}} = \frac{jP_{j,i} + jQ_{j,i}}{\mu_{1,i}^a + \mu_{1,i}^d} \quad (55)$$

Equation (55) can also be written into the following formation:

$$FXY_i(j) = F_{w,i}(j)(\mu_{1,i}^a + \mu_{1,i}^d) = jP_{j,i} + jQ_{j,i} \quad (56)$$

From the population balance eqs. (37)–(39),  $P_j$  and  $Q_j$  can be expressed using mathematical induction:

$$P_{1,i} = \frac{A}{k_p M + k_d - k_f M} e^{-k_f M t} - \frac{A}{k_p M - k_i M} e^{-(k_i M + k_d)t} - A \left( \frac{1}{k_p M + k_d - k_f M} - \frac{1}{k_p M - k_i M} \right) \quad (57)$$

$$P_{2,i} = e^{-(k_p M + k_{tm} M + k_d)t} A k_p M (K_1 e^{(k_p M + k_{tm} M + k_d - k_f M)t} - K_2 e^{(k_p M + k_{tm} M + k_i M)t} - K_3 e^{(k_p M + k_{tm} M + k_d)t} - K) \quad (58)$$

$$Q_{j,i} = \int j(k_{tm} M + k_d) P_{j,i} dt \quad j \geq 2 \quad (61)$$

$$K_1 = \frac{l_1}{k_p M + k_{tm} M + k_d - k_f M} \quad (62)$$

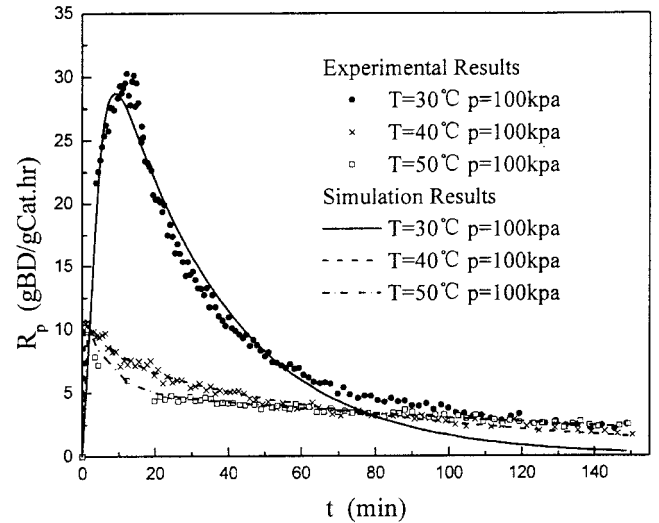


**Figure 5** Fittings of intrinsic model at different reaction temperatures.

**TABLE III**  
Compare with  $M_p$  and  $M_{gas}$

$P$ (atm)	$T$ (°C)	$M_{gas}$ (mol/L)	$M_p$ (mol/L polymer)	Reference
1.0	30	0.039	1.2	7, 12
1.0	40	0.038	1.0	7
1.0	50	0.037	0.86	7
1.4	40	0.054	1.4	7, 12

$$K_2 = \frac{l_2}{k_p M + k_{tm} M - k_i M} \quad (63)$$

$$K_3 = \frac{l_3}{k_p M + k_{tm} M} \quad (64)$$

$$K_4 = l_1 + l_2 - l_3 \quad (65)$$

$$l_1 = A \frac{k_d - k_f M + k_{tm} M}{(k_d M - k_{tm} M)(k_p M + k_d + k_{tm} M - k_f M)} \quad (66)$$

$$l_2 = A \frac{k_{tm} - k_i}{k_i(k_p M + k_{tm} M - k_i M)} \quad (67)$$

$$l_3 = A \frac{(k_i M + k_d - k_f M)k_{tm} M}{k_i M(k_d - k_p M)(k_p M + k_{tm} M)} \quad (68)$$

$$A = \frac{k_i k_f M^2 C_0^*}{k_i M - k_f M + k_d} \quad (69)$$

where  $M$  is equal to  $M_i$  here. From the above equations, the value of  $FXY_i(j)$  of each layer with chain length  $j$  at reaction time  $t$  can be shown.

In the model, the catalyst particle becomes the polymeric particle immediately after the beginning of the reaction. So, the whole polymeric particle, using the fraction of the volume of the particle layer, can show the MWD:

$$\bar{M}_n = \sum_{i=1}^N \frac{V_i \bar{M}_{n,i}}{V_{poly}} \quad (70)$$

$$\bar{M}_w = \sum_{i=1}^N \frac{V_i \bar{M}_{w,i}}{V_{poly}} \quad (71)$$

$$PI = \sum_{i=1}^N \frac{V_i PI_i}{V_{poly}} \quad (72)$$

$$FXY = \sum_{i=1}^N \frac{V_i FXY_i}{V_{poly}} \quad (73)$$

where  $V_i$  is the volume of  $i$ th layer, and  $V_{poly}$ , the volume of the whole polymeric particle.

## PARAMETER VALUES

For the gas-phase polymerization and construction of this model, the key parameters are listed in Table II.  $D_e$  often ranges from  $10^{-11}$  to  $10^{-9}$ . In the model,  $D_e$  is chosen to be  $10^{-11}$ . The diameter of the catalyst particle is 5–100  $\mu\text{m}$ .<sup>11</sup> In the model, 60 and 100  $\mu\text{m}$  are considered.

## RESULTS AND DISCUSSION OF SIMULATION

Simulations were made of the gas-phase polymerization of butadiene. Different chemical and physical factors, such as reaction conditions and transport properties, will affect the kinetics of the gas-phase polymerization of butadiene.

### Effect of temperature

Curves of the decay type were discovered during the reaction. As the reaction temperature increases, the polymerization rate decreases. Fittings of the effect of temperature on the polymerization rate using the kinetic model are shown in Figure 5, which are clearly in good agreement with the experimental results.

From previous research results,<sup>7,9,10</sup> the heat-transfer resistance can be neglected for a low-activity catalyst. So, the temperature in the polymeric particles is almost the same as that in the reactor, that is, the kinetics constants can be used in the all the particle layers from the fitting to the whole polymer particle. The mass transfer in the polymeric particle includes two procedures: sorption on the surface of the particle and transfer in the layers of the particle. In the model, the concentration of the monomer is the sorption con-

**TABLE IV**  
Rate Constants in the Intrinsic Kinetics Model

$T$ (°C)	$k_f$ ( $\times 10^{-4}$ L polymer $\text{mol}^{-1} \text{s}^{-1}$ )	$k_i$ ( $\times 10^{-4}$ L polymer $\text{mol}^{-1} \text{s}^{-1}$ )	$k_p$ ( $\times 10^2$ L polymer $\text{mol}^{-1} \text{Nd s}^{-1}$ )	$k_d$ ( $\times 10^{-3}$ L/s)	$k_{tm}$ ( $\times 10^{-3}$ L polymer $\text{mol}^{-1} \text{s}^{-1}$ )
30	7.29	7.37	2.59	4.37	3.94
40	9.45	9.21	3.54	7.84	5.50
50	9.85	9.82	4.60	8.51	7.61

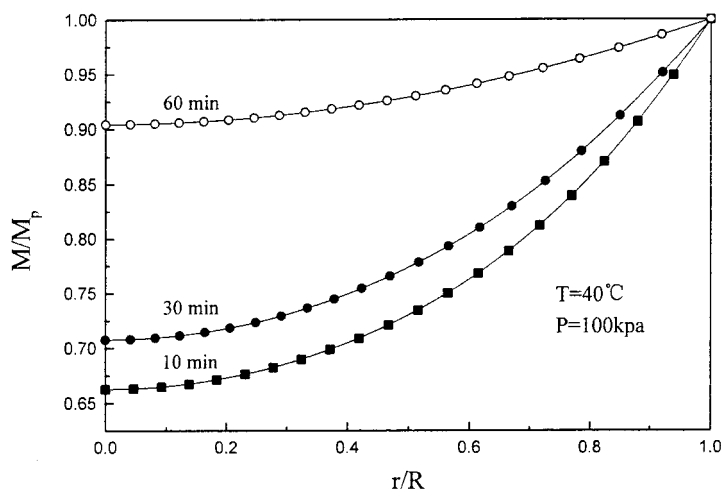


**Figure 6** Simulation of concentration profiles of monomer in the polymeric particle with  $De = 10^{-11} \text{ m}^2/\text{s}$  and  $R_{\text{cat}} = 30 \text{ }\mu\text{m}$ , at  $T = 40^\circ\text{C}$  and  $p = 100 \text{ kPa}$ .

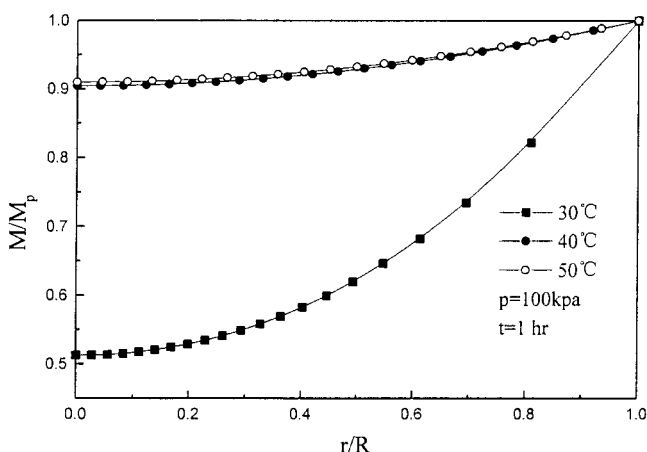
centration listed in Table III. The kinetics constants from the fitting results are shown in Table IV. From Table IV, it can be seen that the  $k_p$  is increased with increase of the temperature. But the influence of deactivation and transfer are also greatly remarkable, which makes the polymerization rate much lower at high temperature. So, the kinetics results do not show that the polymerization rate increases as the reaction temperature increases.

Figure 6 shows the simulations of the concentration profiles of the monomer in the polymeric particle under the condition of  $40^\circ\text{C}$ ,  $100 \text{ kPa}$ . The number of layers ( $N$ ) is 20. After 1 h, the monomer concentration in each layer is almost near to the sorption concentration on the surface of the particle. Figure 7 gives the schematics of the concentration profiles under different reaction conditions. After 1 h from the beginning of the reaction, the concentration of the monomer at  $30^\circ\text{C}$  is lower than that of the others, because of the

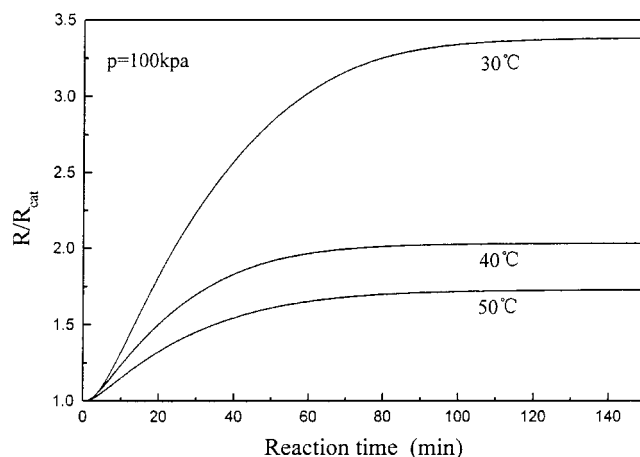
high polymerization rate under the conditions as shown in Figure 2. The profiles of  $40^\circ\text{C}$  and  $50^\circ\text{C}$  are more similar to each other. The reaction at  $40^\circ\text{C}$  and  $50^\circ\text{C}$  is "calm," so the average molecular weight and the MWD of the polymer in the range of both temperatures will not change too much.

Figure 8 shows the particle growth under different reaction temperatures. After quick growth, the curves are almost parallel to the  $x$ -axis, which are the corresponding phenomena to the low reaction rate at a later stage of the reaction. For the low-active catalyst, the volume of the particle is not remarkably changed, which is not greater than  $3.5 R_{\text{cat}}$ .

Figure 9 shows the change of the number-average chain length of the polymer at different reaction times at  $30^\circ\text{C}$ ,  $100 \text{ kPa}$ . The simulations clearly show that the longest chains are produced at the external layer of the particle. As the reaction progresses, the number-average chain length is almost the same in each layer, as



**Figure 7** Simulation of concentration profiles of monomer in the polymeric particle with  $De = 10^{-11} \text{ m}^2/\text{s}$ ,  $R_{\text{cat}} = 30 \text{ }\mu\text{m}$  at  $t = 1 \text{ h}$  at different reaction temperatures and  $100 \text{ kPa}$ .



**Figure 8** Simulation of particle growth at different temperatures at  $p = 100 \text{ kPa}$  ( $De = 10^{-11} \text{ m}^2/\text{s}$ ,  $R_{\text{cat}} = 30 \text{ }\mu\text{m}$ ).

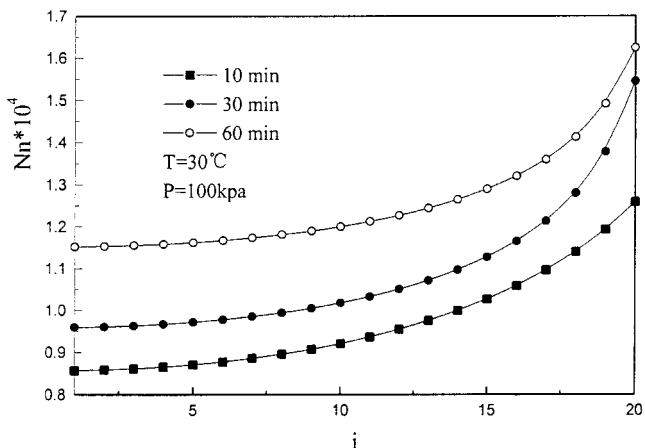


**Figure 9** Simulation of change of number-average chain length in every layer at different times at  $T = 30^\circ\text{C}$  and  $p = 100 \text{ kPa}$  ( $De = 10^{-11} \text{ m}^2/\text{s}$ ,  $R_{\text{cat}} = 30 \mu\text{m}$ ).

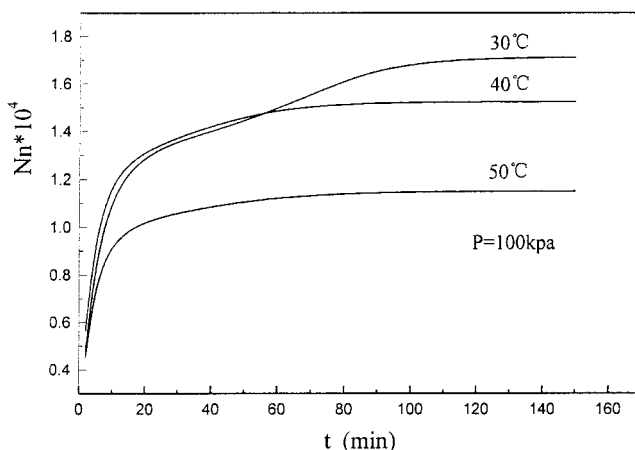
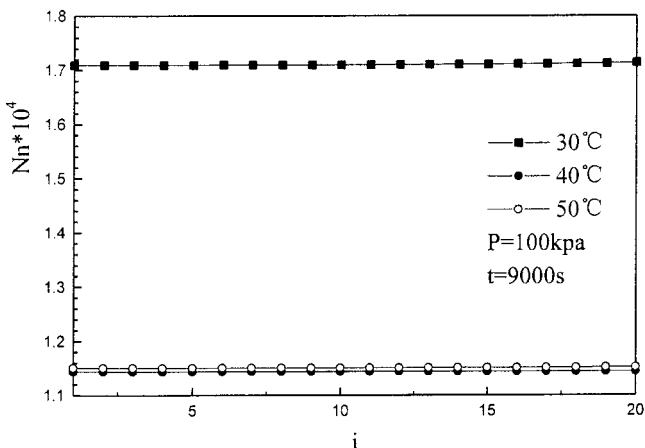


**Figure 11** Simulation of change of overall number-average chain length of whole particle with reaction time at different reaction temperatures and  $p = 100 \text{ kPa}$  ( $De = 10^{-11} \text{ m}^2/\text{s}$ ,  $R_{\text{cat}} = 30 \mu\text{m}$ ).

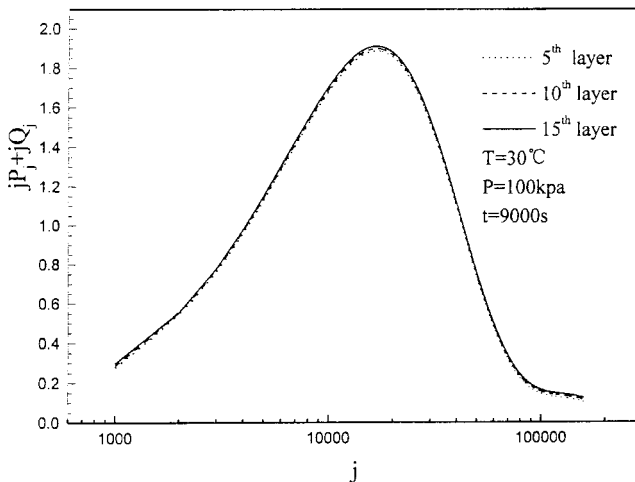
shown in Figure 10. In Figure 10, it can be seen that the number-average chain length in each layer is almost the same under different reaction temperatures when the experiments are finished ( $t = 9000 \text{ s}$ ).

Figure 11 shows simulations of the change of the overall number-average chain length of the polymer as the reaction progresses under different reaction temperatures. The increase of the overall number-average chain length is similar at the beginning of the reaction for all the conditions, but at the later stages of all these reactions, the chain length appears different. Despite the curves being almost parallel to the  $x$ -axis at the later stages, the length of the chain is different. Because of the effect of deactivation and transfer to the monomer, the chain length at  $30^\circ\text{C}$ ,  $100 \text{ kPa}$ , is longer than with the other conditions, as shown in Figure 11. The curve of  $40^\circ\text{C}$  exhibits similarity to that of  $50^\circ\text{C}$  although the height of curves is not same.

Because of the different concentration profiles of the monomer in the polymeric particle, the MWDs in each layer are different. Figure 12 shows the difference at  $30^\circ\text{C}$ ,  $100 \text{ kPa}$ . The chain length is almost the same in each layer, as shown in Figure 12. But at a short reaction time, the MWD in each layer is not the same, as shown in Figure 13. Not only does the fraction of long chains increase, but, also, the MWD moves to the direction of the longer chains. At this time, the concentrations of the monomer of the outer layers are higher than are those of the inner layers. So, the MWD shows a change like that in Figure 13. In fact, at the time when the experiment is finished, the MWD of every layer can be used to represent the MWD of the whole polymeric particle.



**Figure 10** Simulation of number-average chain length in every layer at reaction time  $t = 9000 \text{ s}$  at different reaction temperatures and  $p = 100 \text{ kPa}$  ( $De = 10^{-11} \text{ m}^2/\text{s}$ ,  $R_{\text{cat}} = 30 \mu\text{m}$ ).



**Figure 12** Simulation of different MWDs at different layers of particles when reaction time  $t$  is  $9000 \text{ s}$  and reaction conditions are  $T = 30^\circ\text{C}$  and  $p = 100 \text{ kPa}$  ( $De = 10^{-11} \text{ m}^2/\text{s}$ ,  $R_{\text{cat}} = 30 \mu\text{m}$ ).

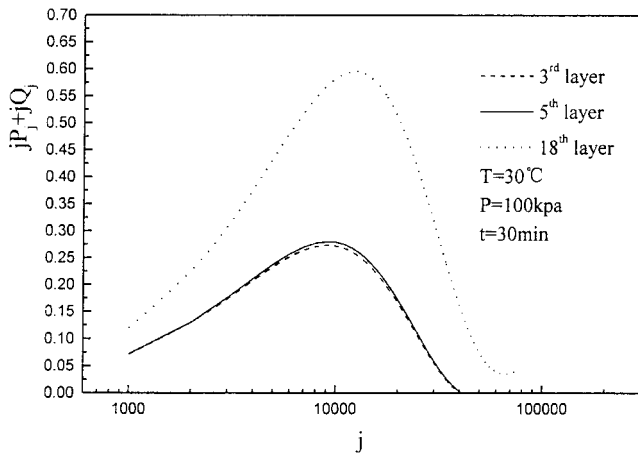


**Figure 13** Simulation of different of MWDs at different layers of particles when reaction time  $t$  is 30 min and reaction conditions are  $T = 30^\circ\text{C}$  and  $p = 100 \text{ kPa}$  ( $De = 10^{-11} \text{ m}^2/\text{s}$ ,  $R_{\text{cat}} = 30 \text{ }\mu\text{m}$ ).

Figure 14 shows simulations of the overall MWD under the different reaction temperatures. At a lower temperature, more long chains are produced. This difference is not remarkable as is the increasing of the temperature. The phenomenon is decided by the deactivation of active sites and the living polymer and the effect of transfer to the monomer at high temperature.

#### Effect of pressure

As the reaction pressure increases, the polymerization rate increases. Figure 15 shows the simulation of the polymerization rate under different reaction pressures. From the kinetics curve shown in Figure 3 and

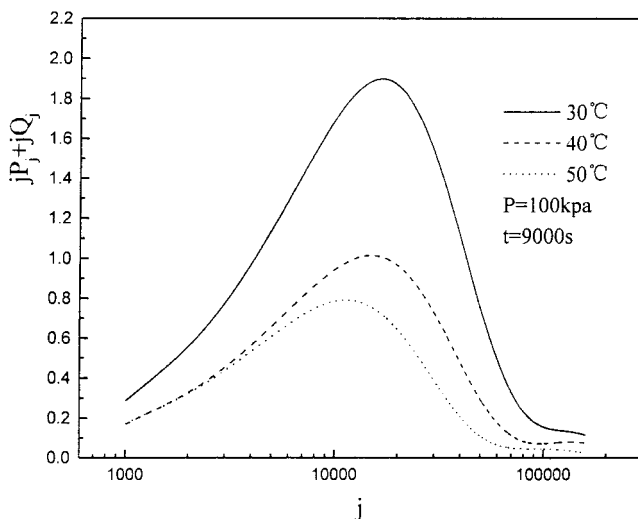


**Figure 14** Simulation of overall MWD of gas-phase polymerization of butadiene under different reaction temperatures and  $p = 100 \text{ kPa}$  after simulation ( $De = 10^{-11} \text{ m}^2/\text{s}$ ,  $R_{\text{cat}} = 30 \text{ }\mu\text{m}$ ), reaction time  $t = 9000 \text{ s}$ ).

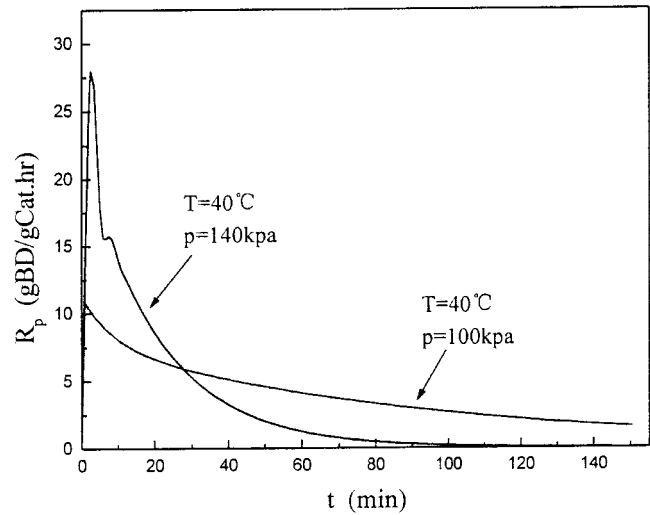


**Figure 15** Simulations of intrinsic model under different reaction pressures.

the simulation, the polymerization rate is almost the same under different reaction pressures at the late stage of the reaction. During the reaction, budadiene also can make active sites deactivate. Under higher pressure, the monomer concentration is higher. Although there is a higher concentration of the monomer at the later stage, a lower concentration of active sites makes the polymerization rate low. But a higher monomer concentration will lead to a broader MWD.

Figure 16 gives schematics of the concentration profiles under different reaction pressures. At high pressure, the concentration of the monomer in the layers is high, leading to the acceleration of the polymerization rate and the high average molecular weight. The polymer chains with a high molecular weight will make the particle larger, as shown in the simulations (Fig. 17). From the simulation, one can see that, although

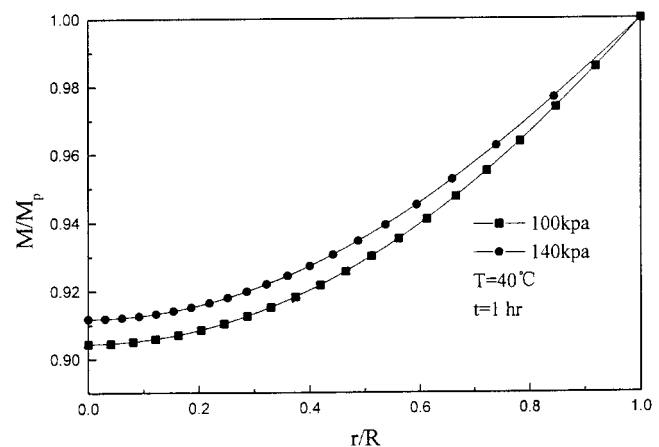


**Figure 16** Simulations of concentration profiles of monomer in the polymeric particle with  $De = 10^{-11} \text{ m}^2/\text{s}$ ,  $R_{\text{cat}} = 30 \text{ }\mu\text{m}$  at  $t = 1 \text{ h}$  at different reaction pressures at  $T = 40^\circ\text{C}$ .

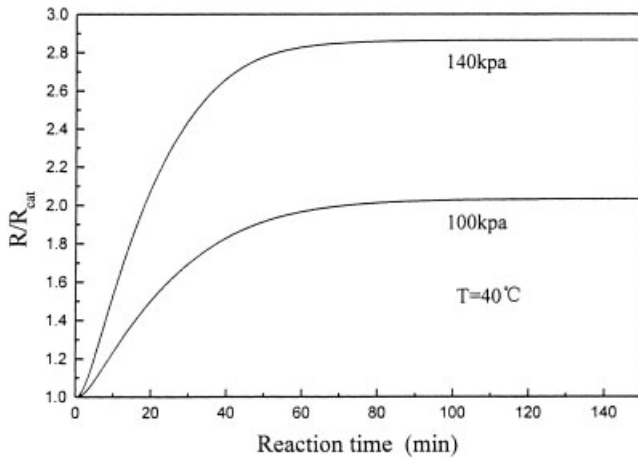
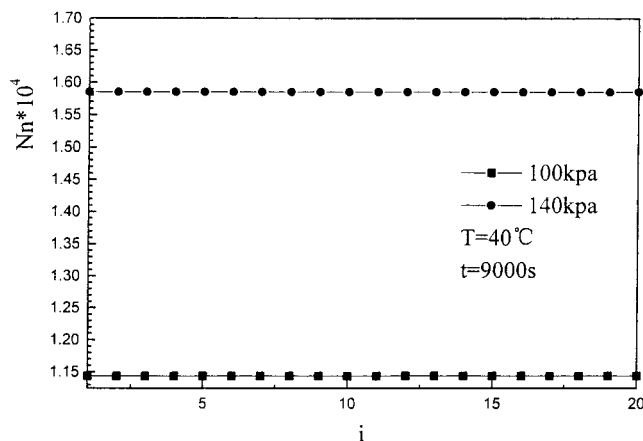


**Figure 17** Simulations of particle growth under different pressures at  $T = 40^\circ\text{C}$  ( $De = 10^{-11} \text{ m}^2/\text{s}$ ,  $R_{\text{cat}} = 30 \mu\text{m}$ ).

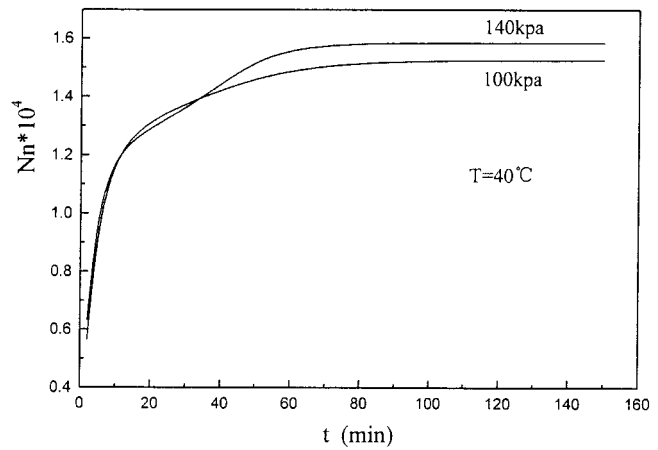
the polymerization rate is almost the same at the later stage, the particle is larger under 140 kPa. This means that the molecular weight and the particle growth are decided at an early stage. From Figure 18, it can be seen that the number-average chain length of the polymer in each layer is almost the same under different reaction pressures when the experiments are finished ( $t = 9000 \text{ s}$ ).

Figure 19 shows the simulation of the change of chain length of the polymer as the reaction progresses under different reaction pressures. The increase of the chain length is similar at the beginning of the reaction for all the conditions, but at the later stages of all these reactions, the chain length appears different.

Figure 20 shows the overall MWD under different reaction pressures. The research has shown that the relationship between the polymerization rate and the reaction pressure is first order,<sup>5</sup> so the reaction pressure in gas-phase polymerization has a great effect on the average molecular weight.



**Figure 18** Simulations of number-average chain length in every layer at reaction time  $t = 9000 \text{ s}$  at different reaction pressures and  $T = 40^\circ\text{C}$  ( $De = 10^{-11} \text{ m}^2/\text{s}$ ,  $R_{\text{cat}} = 30 \mu\text{m}$ ).



**Figure 19** Simulation of change of overall number-average chain length of whole particle with reaction time at different reaction pressures and  $T = 40^\circ\text{C}$  ( $De = 10^{-11} \text{ m}^2/\text{s}$ ,  $R_{\text{cat}} = 30 \mu\text{m}$ ).

**Effect of mass transfer**

Figures 21 and 22 show different profiles of the monomer concentration in the polymeric particle under a larger diffusion coefficient. The profiles of the concentration of the monomer and the particle growth are important to understand the MWD of the gas-phase polymerization of butadiene because it is well known that the average molecular weight and its distribution are related to the monomer concentration and the consuming rate of the monomer.

A larger diffusion coefficient will accelerate the mass transfer. The concentration of the monomer will be larger than that in a small diffusion coefficient. This will lead to a larger molecular weight in a larger diffusion coefficient. The simulation, shown in Figure 23, describes these phenomena.

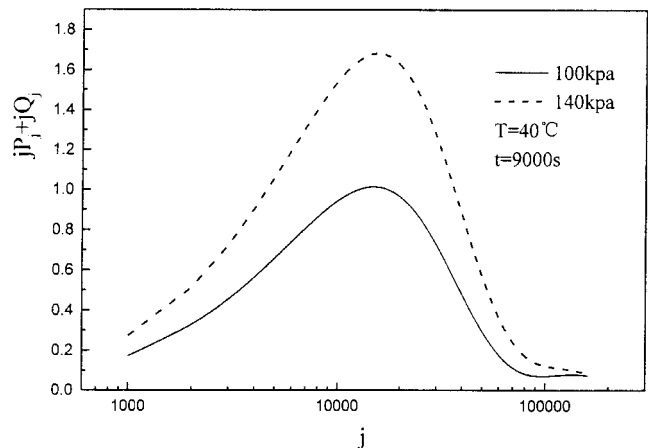


**Figure 20** Simulation of overall MWD of gas-phase polymerization of butadiene at different reaction pressures and  $T = 40^\circ\text{C}$  after simulation ( $De = 10^{-11} \text{ m}^2/\text{s}$ ,  $R_{\text{cat}} = 30 \mu\text{m}$ , reaction time  $t = 9000 \text{ s}$ ).

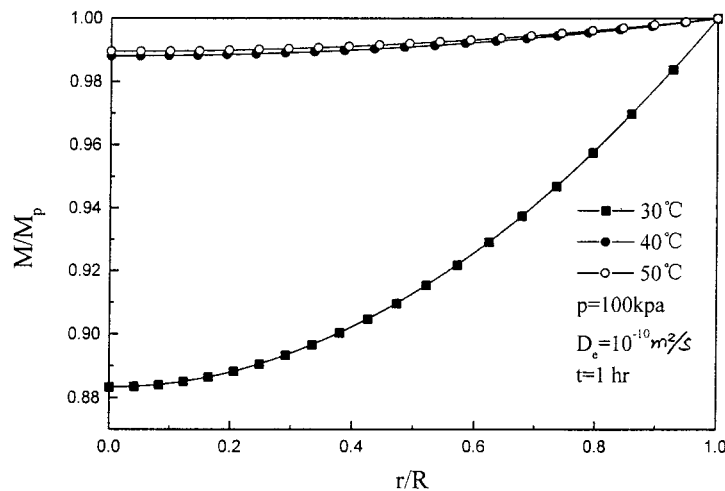


**Figure 21** Simulation of concentration profiles of monomer in the polymeric particle with  $De = 10^{-10} \text{ m}^2/\text{s}$ ,  $R_{\text{cat}} = 30 \text{ }\mu\text{m}$  at  $t = 1 \text{ h}$  at different reaction temperatures and 100 kPa.

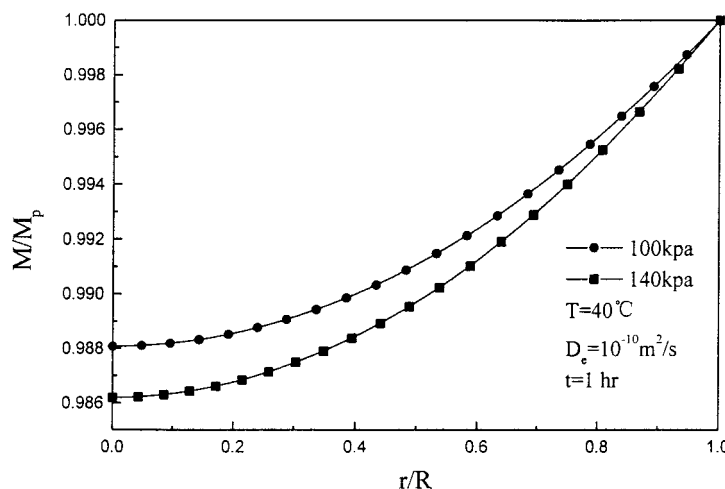
### Effect of catalyst particle size

Figures 24 and 25 show simulations of the particle growth when the radius of the catalyst particle is 50  $\mu\text{m}$ . This will affect the overall MWD at last because the larger size will make mass transfer difficult. Figure 26 shows that the simulation of the average molecular weight when  $R_{\text{cat}}$  is 30  $\mu\text{m}$  is a little larger than that when  $R_{\text{cat}}$  is 50  $\mu\text{m}$ . For the bigger polymeric particle, the transport of the monomer and concentration of the active sites will change.

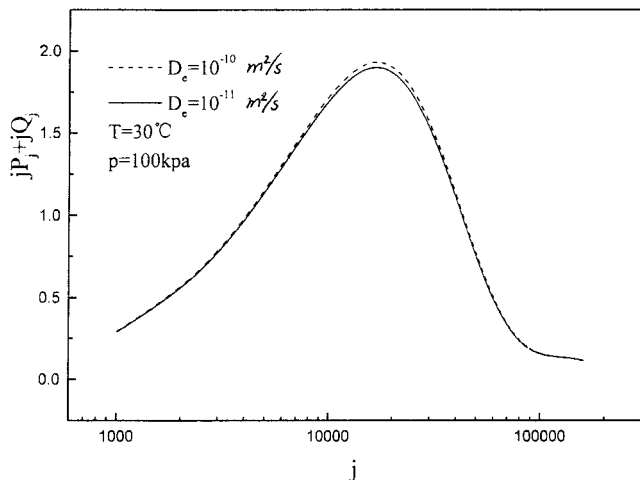
### COMPARISON OF SIMULATION AND EXPERIMENTAL RESULTS

Table V shows a comparison between the simulation results and the experiment results. Figure 27 shows a comparison of the *PI*. The experimental points agree with the simulation points basically in spite of some

difference. Although the number 10's superscripts of simulated molecular weight are coincident with that of the experiment results on the whole, some differences exist at the same time. These differences are perhaps caused mainly by the distribution of the initial concentration of active sites among the catalyst particles. From the dynamic research on the particle growth in the gas-phase polymerization of butadiene,<sup>8</sup> the rates of particle growth are different even if the catalyst particles have the same diameters. This means that the initial concentrations of active sites of the catalyst particles are different from each other, which has a great effect on the MWD of the polymer in the gas-phase polymerization of butadiene. In the model of MWD proposed in this article, the difference of the initial concentration of active sites among the catalyst particles was not considered. The theoretical loading amount of the catalyst was used as the initial concen-



**Figure 22** Simulation of concentration profiles of monomer in the polymeric particle with  $De = 10^{-10} \text{ m}^2/\text{s}$ ,  $R_{\text{cat}} = 30 \text{ }\mu\text{m}$  at  $t = 1 \text{ h}$  at different reaction pressures at  $T = 40^\circ\text{C}$ .



**Figure 23** Simulation of overall MWD of gas-phase polymerization of butadiene at  $T = 30^\circ\text{C}$  and  $p = 100\text{ kPa}$  after simulation ( $De = 10^{-10}\text{ m}^2/\text{s}$ ,  $R_{\text{cat}} = 30\ \mu\text{m}$ ;  $De = 10^{-11}\text{ m}^2/\text{s}$ ,  $R_{\text{cat}} = 30\ \mu\text{m}$ ; reaction time  $t = 9000\text{ s}$ ).

tration of the active sites. Further research should be done to obtain the distribution of the initial concentration of the active sites among the catalyst particles, and then a more accurate model, which can describe the MWD of the gas-phase polymerization of butadiene, might be obtained. From comparison of the *PI*, one can know that the MWD of the gas-phase polymerization of butadiene, in this catalyst system, does not change much under different reaction conditions.

**CONCLUSIONS**

Simulations of the MWD were carried out for the gas-phase polymerization of butadiene. The model is based on the multilayer model of the polymeric particle and new intrinsic kinetics. From the simulations, the following conclusions may be drawn:

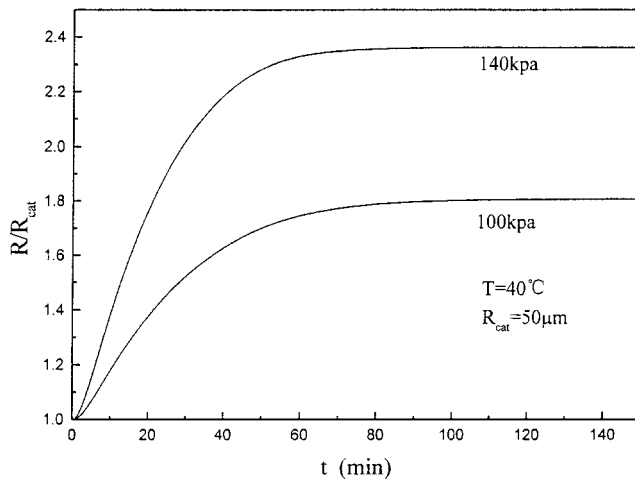


**Figure 25** Simulation of particle growth under different pressures at  $T = 40^\circ\text{C}$  ( $De = 10^{-11}\text{ m}^2/\text{s}$ ,  $R_{\text{cat}} = 50\ \mu\text{m}$ ).

1. The deactivation of active sites of the catalyst and the transfer of polymer chains has a great effect on the intrinsic kinetics and the MWD. At lower temperature, this effect is not so great that large molecular weight averages are obtained.
2. As temperature increases, the average molecular weight decreases; as the reaction pressure increases, the molecular weight averages increase. So, at low temperature and high pressure, polybutadiene with a high average molecular weight can be obtained.
3. In this catalyst system, the *PI* will not change too much under different reaction conditions.

The proposed model can be used to predict the average molecular weight and the MWD of the gas-phase polymerization of butadiene.

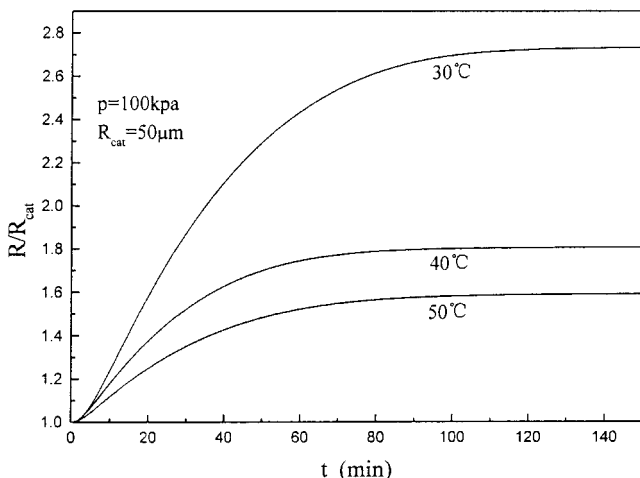


**Figure 24** Simulation of particle growth at different temperatures at  $p = 100\text{ kPa}$  ( $De = 10^{-11}\text{ m}^2/\text{s}$ ,  $R_{\text{cat}} = 50\ \mu\text{m}$ ).

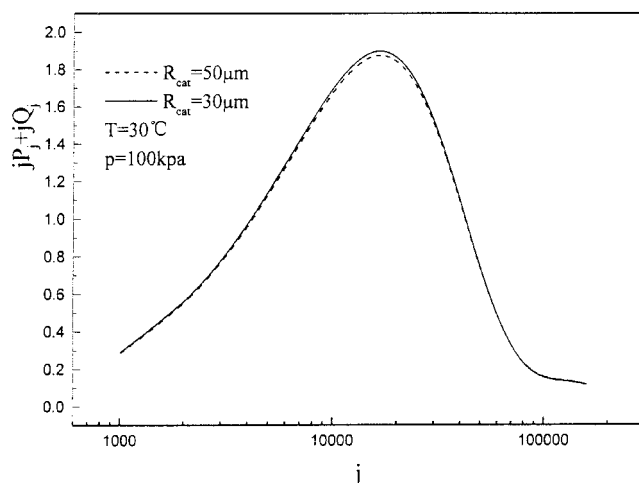


**Figure 26** Simulation of overall MWD of gas-phase polymerization of butadiene under  $T = 30^\circ\text{C}$  and  $p = 100\text{ kPa}$  after simulation ( $De = 10^{-11}\text{ m}^2/\text{s}$ ,  $R_{\text{cat}} = 50\ \mu\text{m}$ ;  $De = 10^{-11}\text{ m}^2/\text{s}$ ,  $R_{\text{cat}} = 30\ \mu\text{m}$ ; reaction time  $t = 9000\text{ s}$ ).

TABLE V  
Compare with the Experiment Results and Simulation Results

	Experimental results			Simulation results		
	$M_n$	$M_w$	$PI$	$M_n$	$M_w$	$PI$
30°C (100 kPa)	$10.3 \times 10^5$	$1.87 \times 10^6$	1.8	$9.2 \times 10^5$	$1.85 \times 10^6$	2.0
40°C (100 kPa)	$5.00 \times 10^5$	$1.06 \times 10^6$	2.1	$6.18 \times 10^5$	$1.24 \times 10^6$	2.0
50°C (100 kPa)	$4.91 \times 10^5$	$1.08 \times 10^6$	2.2	$6.21 \times 10^5$	$1.24 \times 10^6$	2.0
40°C (140 kPa)	$10.5 \times 10^5$	$1.72 \times 10^6$	1.7	$8.6 \times 10^5$	$1.71 \times 10^6$	2.0

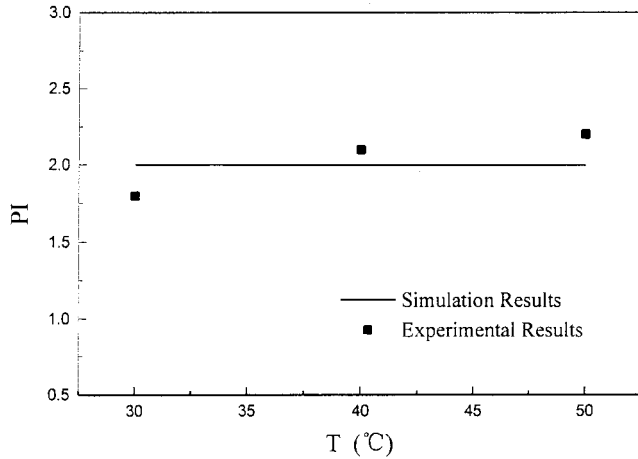


Figure 27 Comparison of  $PI$  of simulation and experimental results.

### NOMENCLATURE

#### Symbol

#### Abbreviation Description

$C^*$	concentration of active sites (mol Nd/g Cat)
$C_0^*$	initial concentration of active sites (mol Nd/g Cat)
$C_{pot}$	potential active sites/concentration of catalyst (mol Nd/g Cat)
$C_d^*$	concentration of deactivated sites (mol Nd/g Cat)
$C_p$	heat capacity of polymer ( $J\ kg^{-1}/K$ )
$C_{pgas}$	heat capacity of monomer gas ( $J\ kg^{-1}/K$ )
$D_e$	molecular diffusion coefficient of butadiene in polybutadiene ( $m^2/s$ )
$d_p$	diameter of polymer particles ( $\mu m$ )
$F_w(j)$	weight-average distribution function
$h$	external film heat-transfer coefficient ( $W\ m^{-2}\ K^{-1}$ )
$i$	$i$ th layer of particle
$IM_i$	concentration of impurity in $i$ th layer
$j$	degree of polymerization
$k$	reaction moment (s)
$k_D$	sorption coefficient when concentration approaches zero [ $L(STP)\ L^{-1}\ polymer\ Pa^{-1}$ ]
$k_e$	effective thermal conductivity of polymer particle ( $W\ m^{-1}\ K^{-1}$ )

$k_d$	deactivation constant (1/s)
$k_f$	constant of formation of active sites ( $L\ polymer\ mol^{-1}\ s^{-1}$ )
$k_{gas}$	thermal conductivity of gas-phase bulk ( $W\ m^{-1}\ K^{-1}$ )
$k_i$	initiation constant of reaction ( $L\ polymer\ mol^{-1}\ s^{-1}$ )
$k_{IM}$	rat constant of reaction with impurity ( $L\ polymer\ mol^{-1}\ s^{-1}$ )
$k_p$	rate constant of propagation ( $L\ polymer\ mol^{-1}\ Nd\ s^{-1}$ )
$k_{tIM}$	rate constant of transfer to impurity ( $L\ polymer\ mol^{-1}\ s^{-1}$ )
$k_{tm}$	rate constant of transfer to monomer ( $L\ polymer\ mol^{-1}\ s^{-1}$ )
$M$	concentration of monomer
$MW$	molecular weight of butadiene monomer ( $kg/mol$ )
$\bar{M}_n$	overall number-average chain length of the whole polymeric particle
$\bar{M}_{n,i}$	number-average chain length in $i$ th layer
$M_p$	sorption concentration of monomer at surface of particle ( $mol/L\ polymer$ )
$\bar{M}_w$	overall weight-average chain length of the whole polymeric particle
$\bar{M}_{w,i}$	weight-average chain length in $i$ th layer
$N$	number of layers
$N_n$	number-average chain length
$N_u$	Nussel number
$p$	reaction pressure (kPa)
$PI$	overall dispersing index of molecular weight
$PI_i$	dispersing index of molecular weight in $i$ th layer
$P_j$	concentration of living polymer ( $mol/m^3\ polymer$ )
$P_r$	Prant number
$Q_j$	concentration of dead polymer ( $mol/m^3\ polymer$ )
$r$	radius of polymeric particle (m)
$R$	radius of outermost layer of particle (m)
$R_{cat}$	radius of catalyst particle (m)
$Re$	Reynolds number
$R_p$	polymerization rate ( $g\ BD\ g^{-1}\ Cat\ h^{-1}$ or $mol\ BD\ mol^{-1}\ Nd\ s^{-1}$ )

$S$	sorption coefficient [ $L(STP) L^{-1} \text{ polymer Pa}^{-1}$ ]
$S_0$	frequency factor of sorption [ $L(STP) L^{-1} \text{ polymer Pa}^{-1}$ ]
$T$	reaction temperature ( $^{\circ}C$ or $K$ )
$t$	reaction time (s)
$T_{\text{gas}}$	temperature of bulk monomer gas ( $^{\circ}C$ or $K$ )
$u$	particle-fluid relative velocity (m/s)
$V_i^k$	volume of $i$ th layer at moment $k$ ( $m^3$ )
$V_{\text{poly}}$	volume of whole particle after reaction ( $m^3$ )
$\Delta H_p$	heat of polymerization (J/mol)
$\Delta t$	time step (s)
$\Delta H_s$	heat of mol sorption (kJ/mol)

### Greek Symbols

$\rho_{\text{gas}}$	density of butadiene gas ( $kg/m^3$ )
$\rho_p$	density of polymeric particle ( $kg/m^3$ )
$\mu_{\text{gas}}$	viscosity of gas phase (Pa s)
$\mu_n^a$	$n$ th moment of living polymer
$\mu_n^d$	$n$ th moment of dead polymer
$\delta$	coefficient of sorption effect [ $L \text{ polymer} / L(STP)$ ]

### References

1. Union Carbide, U.S. Patent 5 728 782, 1998.
2. Ube, Jpn. Patent JP 10 60 020, 1998.
3. Nissim, C.; Joel, M., Jr.; Castner, H. A.; Floyd, K. U.S. Patent 5 859 156, 1999.
4. Eberstein, C.; Garmater, B.; Reichert, K. H.; Sylvester, G. Chem Ingen Technik 1996, 68, 820.
5. Zhao, J. Ph.D. Thesis, Zhejiang University, Hangzhou, 2000.
6. Garmatter, B. M. S. Thesis, Technical University of Berlin, Berlin, 1995.
7. Sun, J.; Eberstein, C.; Reichert, K. H. J Appl Polym Sci 1997, 64, 203.
8. Sun, J.; Zhou, J.; He, S.; Zhao, Q. Chin J Chem Eng 2001, 9, 217.
9. Zhou, J.; Sun, J.; Zhao, Q.; Pan, Z. J Appl Polym Sci 2001, 81, 719.
10. Zhou, J.; Sun, J.; Zhao, Q.; Pan, Z. J Appl Polym Sci 2001, 81, 730.
11. Ni, X. Ph.D. Thesis, Zhejiang University, Hangzhou, 1999.
12. Fang, D. M. S. Thesis, Zhejiang University, Hangzhou, 2001.
13. Soares, J. B. P.; Hamielec, A. E. Polym Reac Eng 1995, 3, 261.
14. Floyd, S.; Choi, K. Y.; Taylor, T. W.; Ray, W. H. J Appl Polym. Sci 1986, 31, 2231.
15. Soares, J. B. P.; Hamielec, A. E. Polymer 1995, 36, 2257.
16. Galvan, R.; Tirrell, M. Chem Eng Sci 1986, 41, 2385.
17. Hu, T. M.S. Thesis, Technical University of Berlin, Berlin, 1995.